# Supplemental Material for "Candidate for a passively protected quantum memory in two dimensions"

The Supplemental Material is organized as follows: In Sec. 1, we provide numerical evidence that the idealized bit flip approximation introduced in the main text is reasonable in the limit of large drive, small single-photon loss, and no dephasing. In Sec. 2, we study a "toy model", which was introduced in the main text, which mimics the dynamics of the 2D photonic-Ising model, and which is tractable both numerically and analytically. This model suggests that leakage out of the codespace arising from single-photon loss and dephasing is not detrimental to passive correction. In Sec. 3, we provide details on the mean-field theory order parameters described in the main text. In Sec. 4 we show that the model studied in the main text can be achieved for an Ising-like Hamiltonian interaction between cavity modes in the presence of the natural system-bath coupling. In Sec. 5 we describe a way to achieve an Ising-like interaction between cavity modes in a superconducting circuit scheme. In Sec. 6, we provide an alternative way of achieving the model in the main text; instead of engineering a Hamiltonian interaction, we describe a way to engineer only the desired dissipators. This scheme relies on the presence of fast unitary gates and ancilla resets.

## 1. IDEALIZED BIT FLIP APPROXIMATION

In this section, we elaborate on the idealized bit flip approximation used in the main text. In experiments, the bit flip error for a single photonic cat qubit is generated via single-photon loss $L_1 = \sqrt{\kappa_1}a$. However, in order to map our many-body-cat-qubit system to the 2D Ising model, we must replace this noise generator with an "idealized bit flip", represented via the jump operator: $E_1 = \sqrt{\kappa_1}aV$ where $V$ is a projector onto the codespace. We provide evidence that $E_1$ is a reasonable approximation for $L_1$ in the limit of small single-photon loss and large two-photon drive (compared to the two-photon loss rate), which is the relevant regime for modern experiments involving photonic cat qubits [1]. We also assume the absence of photon dephasing. To this end, we shall present two models for a single cavity and show that their steady states and dissipative gaps converge in this limit.

Model 1 has the standard single-photon loss term which is expected to appear in experiment. Model 2 has the "idealized bit flip" which is needed to make numerical progress.

*Model 1*: Let us consider a single photonic cavity in the presence of two-photon drive $H = \lambda[a^2 + (a^\dagger)^2]$, two photon loss $L_2 = \sqrt{\kappa_2}a^2$, and single-photon loss $L_1 = \sqrt{\kappa_1}a$. It is convenient to utilize the gauge freedom of the Lindbladian to eliminate the Hamiltonian by incorporating it in a dissipative term. The following two dissipators share the same master equation as the model just described:

$$L_c = \sqrt{\kappa_2}(a^2 - \alpha^2), \qquad \alpha = \sqrt{\frac{\lambda}{\kappa_2}}e^{-i\pi/4} \tag{S1}$$

$$L_1 = \sqrt{\kappa_1}a. \tag{S2}$$

The dissipator $L_c$ will cause states in the Hilbert space to evolve towards the coherent states $|\pm\alpha\rangle$, which are dark states of $L_c$. We thus find that $L_c$ generates the "recovery" part of the Lindbladian, while $L_1$ generates bit flip errors and causes leakage out of the codespace.

From the perspective of quantum trajectories, single-photon loss causes the amplitude of a coherent state to decay due to the non-Hermitian Hamiltonian term proportional to $\kappa_1 a^\dagger a$ which (by itself) causes the coherent state parameter to decay via $\alpha e^{-\kappa_1 t}$. The two-photon drive process ensures that the steady state amplitude remains non-zero, but nevertheless the photon population decreases due to the single-photon loss. Within mean-field theory, the average number $\bar{n}$ of photons in the cavity satisfies

$$\bar{n} = \frac{2\lambda - \kappa_1}{2\kappa_2}. \tag{S3}$$

This suggests that, in the limit of $\lambda/\kappa_2 \gg 1$, the steady state of the system should start to converge to a coherent state $|\pm\mu\rangle$ with a shifted amplitude:

$$a|\pm\mu\rangle = \pm\mu|\pm\mu\rangle, \qquad \mu = \sqrt{\frac{2\lambda - \kappa_1}{2\kappa_2}}e^{-i\pi/4}. \tag{S4}$$

Numerics suggest that the true steady state of the system will be a mixture of several pure states [2]. However, the steady state will have large overlap with the states $|\pm\mu\rangle$. In the limit $\kappa_1/\kappa_2 \ll 1$, the steady state will start to converge to a mixture of the states $|\pm\mu\rangle$.

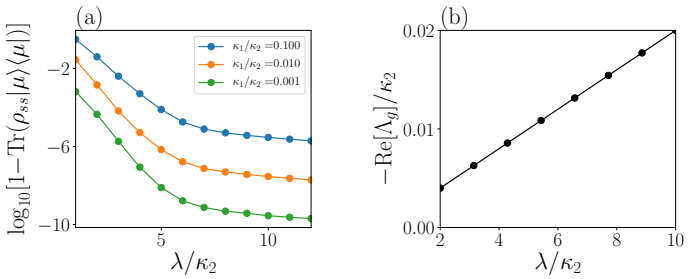


FIG. S1. Model 1: (a) Expectation value of $|\mu\rangle\langle\mu|$ in the steady state of the model described in Eqs. (S1), (S2) with $\lambda/\kappa_2 = N$ for different choices of $\kappa_1/\kappa_2$. In the limit $\lambda/\kappa_2 \gg 1, \kappa_1/\kappa_2 \ll 1$, the system converges to the coherent state $|\mu\rangle$. We use exact Lindblad evolution starting from the initial state $|\alpha\rangle$ and evolving for a time $t = 200/\kappa_2$ to reach the steady state. (b) The dissipative gap $\Lambda_g$ scales linearly as a function of the drive strength, for $\kappa_1/\kappa_2 = 10^{-3}$.

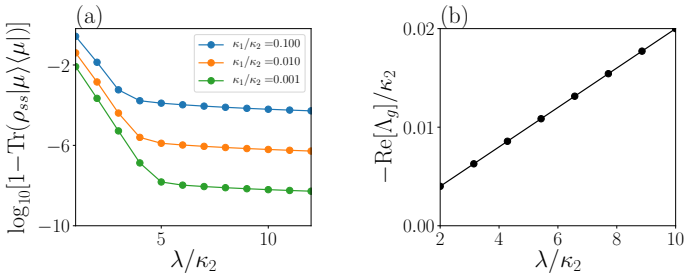


FIG. S2. Model 2: (a) Expectation value of $|\mu\rangle\langle\mu|$ in the steady state of the model described in Eqs. (S6), (S7) with parameters: $\lambda/\kappa_2 = N$ for different choices of $\kappa_1/\kappa_2$. In the limit, $\lambda/\kappa_2 \gg 1, \kappa_1/\kappa_2 \ll 1$ the system converges to the coherent state $|\mu\rangle$. We use exact Lindblad evolution starting from the initial state $|\alpha\rangle$ and evolving for a time $t = 200/\kappa_2$ to reach the steady state. (b) The dissipative gap $\Lambda_g$ scales linearly as a function of the drive strength, for $\kappa_1/\kappa_2 = 10^{-3}$.

We can confirm this via numerical simulations. In Fig. S1 we plot the overlap of the steady state with $|\mu\rangle$ as a function of the drive strength $\lambda/\kappa_2$, for different choices of $\kappa_1/\kappa_2$. We find that the steady state of the system approaches $|\mu\rangle$ in the limit $\lambda/\kappa_2 \gg 1, \kappa_1/\kappa_2 \ll 1$. These parameters are in a regime that is relevant for modern experiments [1]. We also plot the dissipative gap, which scales linearly with the drive strength.

Beyond a shift in the coherent state amplitude, single-photon loss also has the effect of reducing the qubit-steady-state structure to a classical-bit-steady-state structure. Only classical mixtures of coherent states are stable, while off-diagonal coherences have a finite lifetime:

$$\rho_{ss} \approx c|\mu\rangle\langle\mu| + (1-c)|-\mu\rangle\langle-\mu|. \tag{S5}$$

for $c \in [0,1], \lambda/\kappa_2 \gg 1, \kappa_1/\kappa_2 \ll 1$. The steady state is thus two dimensional, enough only to store a classical bit.

*Model 2*: Let us now consider a different model which will have the same steady state and dissipative gap in the limit $\lambda/\kappa_2 \gg 1, \kappa_1/\kappa_2 \ll 1$, but will involve the "idealized bit flip" rather than single-photon loss. Consider the dissipators

$$L_c = \sqrt{\kappa_2}(a^2 - \alpha^2), \qquad \alpha = \sqrt{\frac{\lambda}{\kappa_2}}e^{-i\pi/4} \tag{S6}$$

$$E_1 = \sqrt{\kappa_1}b = \sqrt{\kappa_1}aV, \qquad V = |\alpha_e\rangle\langle\alpha_e| + |\alpha_o\rangle\langle\alpha_o| \tag{S7}$$

where $|\alpha_e\rangle \sim |\alpha\rangle + |-\alpha\rangle, |\alpha_o\rangle \sim |\alpha\rangle - |-\alpha\rangle$. In this model, the dissipator $E_1$ does not cause any leakage of photons out of $|\alpha\rangle$. This is because the non-Hermitian Hamiltonian term proportional to $E_1^\dagger E_1$ keeps superpositions of $|\pm\alpha\rangle$ in this subspace (due to the projector $V$). Nevertheless, the term $E_1$ ensures that quantum superpostions of $|\pm\alpha\rangle$ are unstable, while classical mixtures are stable. The steady state starts to converge to the following state in the limit of large drive $\lambda/\kappa_2 \gg 1$:

$$\rho_{ss} \approx c|\alpha\rangle\langle\alpha| + (1-c)|-\alpha\rangle\langle-\alpha|, \tag{S8}$$

for $c \in [0, 1]$.

The overlap between $|\alpha\rangle$ and $|\mu\rangle$ satisfies

$$|\langle\alpha|\mu\rangle|^2 = \exp\left[-\frac{\kappa_1^2}{16\kappa_2\lambda}\right] \approx 1 - \frac{\kappa_1^2}{16\kappa_2\lambda} + \dots \tag{S9}$$

This implies that the deviation from unity scales as $\kappa_1^2$ when $\kappa_2\lambda \gg \kappa_1^2$. We confirm this in Fig. S2: The deviation between the steady state of Model 2 and $|\mu\rangle$ scales quadratically with $\kappa_1$ in the limit of large drive. We also plot the dissipative gap, which again scales linearly with the drive strength.

We have shown that Models 1 and 2 converge to each other in terms of their steady state and their dissipative gap in the limit $\lambda/\kappa_2 \gg 1, \kappa_1/\kappa_2 \ll 1$. This suggests that Model 2 is a reasonable approximation for Model 1 in this regime. Intuitively, this happens because the system quickly evolves toward the codespace, such that the projector term $V$ acts trivially on the state. In the main text, we demonstrated that Model 2 passively corrects against bit flip errors via the Ising-like dissipators described above. We expect Model 1 to behave in qualitatively the same manner after the replacement of $b \to a$.

We note that, although we used the limit $\lambda/\kappa_2 \gg 1, \kappa_1/\kappa_2 \ll 1$ to establish the exact mapping to the Ising model, we do not expect that this limit is needed to preserve quantum information in general. Rather, the system only needs to stay within the ordered phase (see Fig. 3 in the main text and SM Sec. 3). A relatively small $\kappa_1$ ensures that the steady state of the dynamics is a mixed state. Nevertheless, we expect that this mixed state will be a "noiseless subsystem", which implies that it can be decoded with a channel superoperator at the end of the dynamics.

## 2. TOY MODEL

The Ising-inspired bit-flip recovery jump operators [Eqs. (9) in the main text] by themselves will not give rise to protection against single-photon loss in the absence of a drive, since single-photon loss will cause the system to evolve to a vacuum state. In this section, we argue that, when the bit-flip recovery is coupled with the driving, the resulting environment is able to protect against both dephasing and single-photon loss errors.

Ideally, we would like to numerically simulate the 2D array of $M^2$ cat qubits introduced in the main text. However, such a simulation is computationally expensive. We restrict ourselves to the toy model introduced in the main text: a single cat qubit coupled to a two-level system, the latter described by Pauli operators $X, Y, Z$. The logical states of this toy system are defined as $|\downarrow\rangle|\alpha_o\rangle$ and $|\downarrow\rangle|\alpha_e\rangle$, where $|\alpha_e\rangle, |\alpha_o\rangle$ are the logical states for a single cat qubit. The noise and recovery jump operators are modified to

$$l_c = \sqrt{\kappa_2}(a^2 - \alpha^2), \qquad \alpha = \sqrt{\frac{\lambda}{\kappa_2}}e^{-i\pi/4} \tag{S10}$$

$$l_1 = \sqrt{\kappa_1}Xa, \quad l_d = \sqrt{\kappa_d}a^\dagger a, \tag{S11}$$

$$l_{nn} = \sqrt{\kappa_{nn}}\frac{1}{2}X(1 - Z)a, \tag{S12}$$

where $l_c$ generates a Lindbladian that is equivalent to the combined action of $h$ and $l_2$ in the main text. In this toy model, the spin-1/2 particle is essentially a "classical bit" that takes the discrete value of up or down. Any single-photon loss event is always accompanied by a flip of the spin. A bit-flip recovery for the cat qubit can then be achieved by checking the orientation of the spin: an annhilation operator $a$ is applied to the cavity if the spin points upwards, otherwise nothing happens. This mimics the full 2D case where a bit-flip recovery jump is triggered by a parity misalignment between nearest-neighbor cat qubits. The difference between the 2D model and the toy model is that the latter always knows when an odd number of single photon-loss events has occurred. What remains to be tested is whether the errors can be corrected by introducing the bit-flip recovery jump.

Suppose we initialize the dynamics with a generic state in the codespace. We consider the following two scenarios: We choose the model with (i) $\kappa_2 = 1, \kappa_d = 0.1, \kappa_1 = 0.1, \kappa_{nn} = 0$ and (ii) $\kappa_2 = 1, \kappa_d = 0.1, \kappa_1 = 0.1, \kappa_{nn} = 0.3$. The system size parameter is $N = \lambda/\kappa_2$ with $N \to \infty$ representing the thermodynamic limit. The initial state is first evolved with this Lindbladian for duration $T = 15$, then followed by the corresponding noiseless Lindbladian evolution ($\kappa_d = \kappa_1 = 0$) for another $T = 15$. In the end, we compute the fidelity between the final state and the initial state. The results for the two scenarios are shown in Fig. S3 for different $N$.

The results clearly show distinct behaviors. For case (i), where $\kappa_{nn} = 0$, the single-photon loss causes uncorrectable errors in the stored memory, leading to a saturated fidelity of 1/2 (due to an equal mixture of the flipped and unflipped

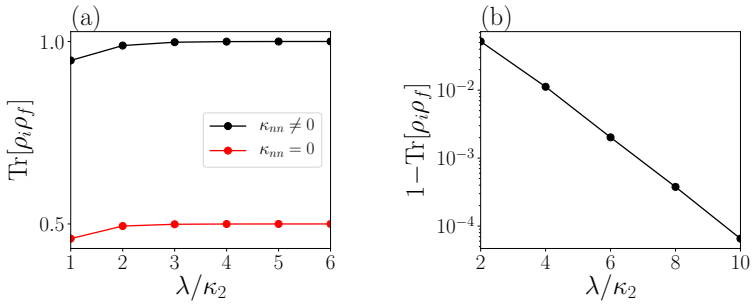


FIG. S3. We initialize the dynamics with state $\rho_i = |\psi\rangle\langle\psi|$, where $|\psi\rangle = \frac{1}{\sqrt{5}}|\downarrow\rangle|\alpha_e\rangle + \frac{2e^{i\pi/4}}{\sqrt{5}}|\downarrow\rangle|\alpha_o\rangle$. (a) Overlap between the initial and final states for $\kappa_{nn} = 0$ [case (i)] and $\kappa_{nn}/\kappa_2 = 0.3$ [case (ii)] as $N = \lambda/\kappa_2$ increases. Parameters: $\kappa_d/\kappa_2 = 0.1, \kappa_1/\kappa_2 = 0.1$. (b) For case (ii), i.e. $\kappa_{nn} \neq 0$, the log scale plot shows that the fidelity converges exponentially quickly to 1 as $N \to \infty$.

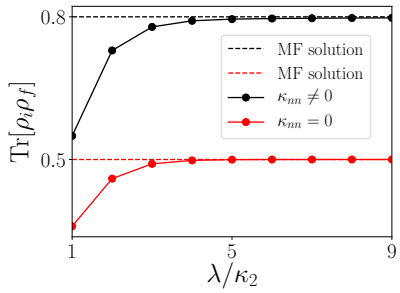


FIG. S4. Repeating the same simulation as in Fig. S3, except the recovery (noiseless) Lindblad evolution is done using $\kappa_{nn} = \kappa_d = \kappa_1 = 0$ in both cases (i) and (ii) [not just case (i)]. The overlap between the initial and final states is larger than 1/2 when $\kappa_{nn} \neq 0$ during the noisy dynamics [modified case (ii)], while the overlap saturates to 1/2 when $\kappa_{nn} = 0$ [the original case (i)]. In the thermodynamic limit, the overlap values agree with mean-field results (shown as horizontal dashed lines).

states) as $N$ increases. For case (ii), where $\kappa_{nn} \neq 0$, increasing $N$ leads to a fidelity exponentially close to the ideal value of 1.

As a sanity check, let us consider the same numerical simulation but modify case (ii) by setting $\kappa_{nn} = 0$ during the noiseless dynamics (while still keeping $\kappa_{nn} = 0.3$ during the noisy dynamics). The results of the simulation are shown in Fig. S4. In case (i), which is identical to the one studied in Fig. S3, the fidelity relaxes to 1/2 regardless of the system size as before. The modified case (ii) shows a saturated fidelity between 1/2 and 1, suggesting a partial preservation of the initial quantum memory. This again confirms the dynamical quantum memory protection arising from the flip-recovery jump and two-photon drive.

**Mean-field analysis of the toy model.**—We use a mean field approach to show that, despite the spin-boson coupling in our toy model, the $\mathbb{Z}_2$ symmetry-breaking phase diagram of the single cat qubit is reproduced. Given an observable $\hat{O}$ and a Lindbladian term $\mathcal{L}$ generated by the jump operator $L$, the expectation value obeys

$$\mathrm{Tr}\left[\hat{O}\mathcal{L}\rho\right] = -\frac{1}{2}\,\mathrm{Tr}\left[[\hat{O}, L^\dagger]L\rho + L^\dagger[L, \hat{O}]\rho\right]. \tag{S13}$$

Using this, we can derive a coupled set of mean-field equations of motion for $\langle a\rangle$ and $\langle Z\rangle$:

$$\frac{d}{dt}\langle a\rangle = -i\lambda\langle a^\dagger\rangle - \frac{1}{2}\left(\kappa_1 + \kappa_d + \frac{\kappa_{nn}}{2}(1 - \langle Z\rangle)\right)\langle a\rangle - \kappa_2|\alpha|^2\langle a\rangle, \tag{S14}$$

$$\frac{d}{dt}\langle Z\rangle = -2\kappa_1|\alpha|^2\langle Z\rangle + \kappa_{nn}|\alpha|^2(1 - \langle Z\rangle). \tag{S15}$$

This yields the mean-field fixed point solutions for both observables

$$\langle Z\rangle = \frac{\kappa_{nn}}{\kappa_{nn} + 2\kappa_1}, \tag{S16}$$

$$\kappa_2|\alpha|^2 = |\lambda| - \frac{1}{2}\left(\kappa_1 + \kappa_d + \frac{\kappa_1\kappa_{nn}}{\kappa_{nn} + 2\kappa_1}\right). \tag{S17}$$

The expression closely matches the simulation in the thermodynamic limit (see Fig. S4).

It is interesting to note that if $\kappa_1/\kappa_2$ is small enough, then any non-zero $\kappa_{nn}$ can give rise to a stable memory ($\langle Z\rangle, \langle a\rangle \neq 0$). On the other hand, if $\kappa_1/\kappa_2$ is large, a large $\kappa_{nn}$ can destabilize the memory, leading to $\langle a\rangle = 0$.

## 3. MEAN-FIELD SOLUTION FOR THE 2D PHOTONIC-ISING MODEL

In this section, we present the mean-field solution for the 2D photonic-Ising model. The mean-field analysis shows the existence of two symmetry-breaking transitions via two order parameters: $a^2$ and $Q \equiv e^{i\pi a^\dagger a}$.

We consider a product-state mean-field ansatz $\rho = \bigotimes_{x,y=1}^{M} \rho_{x,y}$. At each site, $\rho_{x,y}$ is a density matrix for a two-level system in the basis of $|\pm\alpha_{MF}\rangle$ for some coherent parameter $\alpha_{MF}$. We first begin by deriving the mean-field equation for $Q = e^{i\pi a^\dagger a}$. Note that all the terms that commute with $Q$ do not contribute to the time evolution. We are therefore left to consider only the single-photon loss term and the bit-flip correction term. Using Eq. (S13), we obtain

$$\frac{d\langle Q\rangle}{dt} = -2\left(\kappa_1\langle a^\dagger a Q\rangle + \kappa_{nn}\langle a^\dagger a Q P_{\kappa_{nn}}\rangle + \tilde{\kappa}_{nn}\langle a^\dagger a Q P_{\tilde{\kappa}_{nn}}\rangle\right), \tag{S18}$$

where $P_{\kappa_{nn}}, P_{\tilde{\kappa}_{nn}}$ are sums of projectors onto different parity configurations with rates $\kappa_{nn}, \tilde{\kappa}_{nn}$, as introduced in the main text. Within mean-field theory, we replace the expectations by a product of expectations at each site, yielding

$$-\frac{1}{2|\alpha|^2}\frac{d\langle Q\rangle}{dt} = \frac{\kappa_{nn} - 4\tilde{\kappa}_{nn}}{16}\langle Q\rangle^5 + \frac{\kappa_{nn} + 4\tilde{\kappa}_{nn}}{8}\langle Q\rangle^3 - \left(\frac{3\kappa_{nn} + 4\tilde{\kappa}_{nn}}{16} - \kappa_1\right)\langle Q\rangle. \tag{S19}$$

Similarly, we can derive the mean-field equation for $a^2$:

$$\frac{d\langle a^2\rangle}{dt} = -\kappa_2(2\langle a^\dagger a a^2\rangle + \langle a^2\rangle) - i\lambda(2\langle a^\dagger a\rangle + 1) - \kappa_1\langle a^2\rangle - 2\kappa_d\langle a^2\rangle - \kappa_{nn}\langle a^2 P_{\kappa_{nn}}\rangle - \tilde{\kappa}_{nn}\langle a^2 P_{\tilde{\kappa}_{nn}}\rangle. \tag{S20}$$

With the mean-field ansatz, we may approximate $\langle a^\dagger a a^2\rangle \approx |\alpha_{MF}|^2\langle a^2\rangle$. We also have $\langle a^2 P_{\tilde{\kappa}_{nn}}\rangle = \langle a^2\rangle\langle P_{\tilde{\kappa}_{nn}}\rangle$ and $\langle a^2 P_{\kappa_{nn}}\rangle = \langle a^2\rangle\langle P_{\kappa_{nn}}\rangle$. After some algebra, the mean-field fixed points at the thermodynamic limit (e.g. $\kappa_2 \to 0$) can be found to satisfy

$$\langle Q\rangle^2 = \frac{2\sqrt{\kappa_{nn}^2 - 4\kappa_1(\kappa_{nn} - 4\tilde{\kappa}_{nn})} - \kappa_{nn} - 4\tilde{\kappa}_{nn}}{\kappa_{nn} - 4\tilde{\kappa}_{nn}}, \tag{S21}$$

$$|\alpha_{MF}|^2 = \frac{2\lambda - \kappa_1 - 2\kappa_d - \gamma_4\langle Q\rangle^4 - \gamma_2\langle Q\rangle^2 - \gamma_0}{2\kappa_2}, \tag{S22}$$

where $\gamma_4 = (-3\kappa_{nn} + 4\tilde{\kappa}_{nn})/16$, $\gamma_2 = (\kappa_{nn} - 4\tilde{\kappa}_{nn})/8$, and $\gamma_0 = (\kappa_{nn} + 4\tilde{\kappa}_{nn})/16$. In addition, $\langle Q\rangle^2 \neq 0$ is only possible when $|\alpha_{MF}|^2 \neq 0$. Intuitively, when $\langle a^2\rangle = 0$, the cavity will lose coherence and decay to the vacuum due to the noise. The logical states are no longer well-defined in this case.

It is important to note that the mean-field solution suggests that the leakage caused by both finite $\kappa_1$ and finite $\kappa_d$ is compensated by the two-photon drive. The effect of this leakage amounts to a shift in the steady state coherent parameter.

## 4. A MICROSCOPIC DERIVATION OF THE PHOTONIC-ISING DISSIPATORS

Here we establish an explicit connection between the Hamiltonian approach for the photonic-Ising model and the microscopic Lindbladian approach. This section (Section 4) provides an example where the proposed photonic-Ising dissipators emerge naturally from a microscopic coupling, unlike the example in the previous section. In the next section (Section 5), we will discuss an experimental protocol that realizes the desired Hamiltonian coupling based on superconducting circuits.

### The microscopic generators

Let us start by considering a microscopic Hamiltonian of both the system and the bath:

$$H = H_S + H_B + H_{SB}, \tag{S23}$$

where $H_S = -J\sum_{\langle i,j\rangle} Q_iQ_j$, and $H_B, H_{SB}$ are the bath and the system-bath coupling Hamiltonian, respectively. Notice that, in contrast to the main text, we explicitly introduced an energy scale $J > 0$ in $H_S$ to help us carry out the analysis. We consider $H_{SB} = \sum_i (a_i + a_i^\dagger) \otimes B_i$, where $a_i$ is the annihilation operator on the photonic-Ising lattice and $B_i$ is some Hermitian local operator on the bath. We assume that the bath is large and the interaction $H_{SB}$ is weak such that effects of the coupling on the bath is fast and can be neglected, i.e. the full density matrix approximately factorizes into a product of a system density matrix and a bath density matrix: $\rho(t) \approx \rho_S(t) \otimes \rho_B$, $\forall t$. Provided that the standard Born-Markov approximation (i.e. the smallness of the influence of the system-bath coupling on the bath) and the rotating-wave approximation are valid [3], we can derive the Master equation in the interaction picture as

$$\frac{d\rho_S}{dt} = -i[H', \rho_S] + \sum_\omega \sum_{i,j} \gamma_{i,j}(\omega) \left( A_i(\omega)\rho_S A_j^\dagger(\omega) - \frac{1}{2}\{A_j^\dagger(\omega)A_i(\omega), \rho_S\} \right). \tag{S24}$$

Here $H'$ is the Lamb-shift Hamiltonian which we will define below. The operator $A_i(\omega)$ is defined as

$$A_i(\omega) = \sum_E \Pi(E)(a_i + a_i^\dagger)\Pi(E + \omega), \tag{S25}$$

where $\Pi(E)$ is a projection the eigenstates of $H_S$ of energy E. So $A_i(\omega)$ is a lowering operator: it is the part of $a_i + a_i^\dagger$ that couples eigenstates of $H_S$ whose energies differ by $\omega$. It is easy to verify that $\sum_\omega A_i(\omega) = a_i + a_i^\dagger$. Note that $a_i + a_i^\dagger$ can only create an energy difference of $\omega = 0, \pm 4J, \pm 8J$, and we can work out $A_i(\omega)$ for each case explicitly.

It is straightforward to verify that $A_i(\omega)$ is geometrically local and takes the form

$$A_i(0) = (a_i + a_i^\dagger)\sum_{\sigma(2)} P_{\sigma(2)}, \;\; A_i(0) = (a_i + a_i^\dagger)\sum_{\sigma(2)} P_{\sigma(2)}, \tag{S26}$$

$$A_i(+4J) = (a_i + a_i^\dagger)\sum_{\sigma(3)} P_{\sigma(3)}, \;\; A_i(-4J) = (a_i + a_i^\dagger)\sum_{\sigma(1)} P_{\sigma(1)}, \tag{S27}$$

$$A_i(+8J) = (a_i + a_i^\dagger)\sum_{\sigma(4)} P_{\sigma(4)}, \;\; A_i(-8J) = (a_i + a_i^\dagger)\sum_{\sigma(0)} P_{\sigma(0)}, \tag{S28}$$

where $P_{\sigma(n)}$ denotes the projector onto different local configurations $\sigma(n)$ around site $i$ with $n$ domain walls. The following relationship is satisfied: $A_i^\dagger(\omega) = A_i(-\omega)$.

In Eq. (S24), the Hamiltonian $H'$ is the Lamb-shift Hamiltonian

$$H' = \sum_\omega \sum_{i,j} \chi_{i,j}(\omega) A_i^\dagger(\omega) A_j(\omega), \tag{S29}$$

where the coupling $\chi_{i,j}(\omega)$ is given in terms of the Fourier transform of the reservoir correlation functions [3]:

$$\chi_{i,j}(\omega) = \mathrm{Im}\{C_{i,j}(\omega)\}, \text{ where } C_{i,j}(\omega) \coloneqq \int_0^\infty ds e^{i\omega s} \langle B_i^\dagger(s) B_j(0)\rangle, \tag{S30}$$

where $B_i^\dagger(s)$ denotes Heisenberg evolution under $H_B$ for time $s$ and the expectation value is taken in the initial thermal state of the bath. To simplify the expression, we make the assumption that $\langle B_i^\dagger(s)B_j(0)\rangle \approx \langle B_i^\dagger(s)\rangle\langle B_j(0)\rangle$ for $i \neq j$. In particular, this is immediately satisfied if each site is coupled to its own bath. Note that we also assumed $\langle B_i^\dagger(s)\rangle = \langle B_j(0)\rangle = 0$ in order to get to Eq. (S24) (see Ref. [3]). We find $\chi_{i,j}(\omega) = 0$ for $i \neq j$. Defining $\chi_{i,i}(\omega) \coloneqq \chi_i(\omega)$, $H'$ simplifies to

$$\begin{aligned} H' &= \sum_{\omega,i} \chi_i(\omega) A_i^\dagger(\omega) A_i(\omega) \\ &= \sum_i \left( \sum_\omega \chi_i(\omega) \sum_{\sigma(n[\omega])} P_{\sigma(n[\omega])} \right) (a_i + a_i^\dagger)^2, \end{aligned} \tag{S31}$$

where $n[\omega]$ is the number of domain walls in the projected configuration as in Eqs. (S26)-(S28). We therefore have a Hamiltonian contribution quadratic in the bosonic operators. A Hamiltonian of this form will in general

cause dephasing of the quantum memory. However, such an effect will be exponentially suppressed in $|\alpha|^2$ by the combination of two-photon drive and two-photon loss in Eq. (8) of the main text.

In Eq. (S24), the dissipative rate $\gamma_{i,j}(\omega)$ is also expressed in terms of the correlation functions as $\gamma_{i,j}(\omega) = \mathrm{Re}[C_{i,j}(\omega)] = \int_{-\infty}^{\infty} ds e^{i\omega s}\langle B_i^\dagger(s)B_j(0)\rangle$. We make use of the locality assumption again so $\gamma_{i,j} = 0$ for $i \neq j$. The master equation Eq. (S24) simplifies to

$$\frac{d\rho_S}{dt} = -i[H', \rho_S] + \sum_{\omega\in\{0,\pm 2J,\pm 4J\}} \sum_i \gamma_i(\omega)\left(A_i(\omega)\rho_S A_i^\dagger(\omega) - \frac{1}{2}\{A_i^\dagger(\omega)A_i(\omega), \rho_S\}\right). \tag{S32}$$

Imposing the Kubo-Martin-Schwinger (KMS) condition (i.e. assuming that the bath is in thermal equilibrium [3]) leads to the detailed balance relation

$$\gamma_i(\omega) = e^{\beta\omega}\gamma_i(-\omega). \tag{S33}$$

for some temperature $\beta = 1/(k_B T)$ set by the bath.

### Recovering the photonic-Ising dissipators

We now show that the photonic-Ising dissipators defined in Eq. (9) of the main text are a special case of the dissipative part of Eq. (S32). Let us set $\gamma(0) = \gamma(-4J) = \gamma(-8J) = \kappa_1/2$. This can be satisfied at low temperature for a roughly constant density of states across this energy range. Suppose we initialize the system $\rho_S(0)$ as a pure state corresponding to a well-defined domain-wall configuration. Let us denote $\mathcal{D}(L)[\rho_S] = L\rho_S L^\dagger - \frac{1}{2}\{L^\dagger L, \rho_S\}$, then, for any site $i$ and time $t$, the density matrix $\rho_S(t)$ satisfies

$$\mathcal{D}\left(a_i \sum_\sigma P_\sigma\right)[\rho_S] = \sum_\sigma \mathcal{D}(a_i P_\sigma)[\rho_S], \tag{S34}$$

where the sum is taken over some projector $P_\sigma$ that projects onto distinct domain wall configuration $\sigma$. The same result holds when we replace $a_i$ by $a_i^\dagger$ or $a_i + a_i^\dagger$. This is because $\rho_S(t)$ evolved under Eq. (S32) is always a linear combination of some $|\psi_1\rangle\langle\psi_2|$, where $|\psi_1\rangle, |\psi_2\rangle$ might be different states but they are always the same domain wall configuration defined by the parity misalignment. The dissipative terms on site $i$ in Eq. (S32) now read

$$\begin{aligned}
&\gamma_i(0)\mathcal{D}(A_i(0))[\rho_S] + \sum_{\omega=\pm 4J}\gamma_i(\omega)\mathcal{D}(A_i(\omega))[\rho_S] + \sum_{\omega=\pm 8J}\gamma_i(\omega)\mathcal{D}(A_i(\omega))[\rho_S] \\
&= \frac{\kappa_1}{2}\sum_{\omega=0,\pm 4J,\pm 8J}\mathcal{D}(A_i(\omega))[\rho_S] + \left(\gamma_i(2J) - \frac{\kappa_1}{2}\right)\mathcal{D}(A_i(4J))[\rho_S] + \left(\gamma_i(8J) - \frac{\kappa_1}{2}\right)\mathcal{D}(A_i(8J))[\rho_S] \\
&= \frac{\kappa_1}{2}\mathcal{D}\left(\sum_{\omega=0,\pm 4J,\pm 8J} A_i(\omega)\right)[\rho_S] + \frac{\kappa_1}{2}(e^{4\beta J}-1)\mathcal{D}(A_i(4J))[\rho_S] + \frac{\kappa_1}{2}(e^{8\beta J}-1)\mathcal{D}(A_i(8J))[\rho_S] \\
&= \frac{\kappa_1}{2}\mathcal{D}(a_i + a_i^\dagger)[\rho_S] + \frac{\kappa_1}{2}(e^{4\beta J}-1)\sum_{\sigma(3)}\mathcal{D}((a_i + a_i^\dagger)P_{\sigma(3)})[\rho_S] + \frac{\kappa_1}{2}(e^{8\beta J}-1)\sum_{\sigma(4)}\mathcal{D}((a_i + a_i^\dagger)P_{\sigma(4)})[\rho_S].
\end{aligned} \tag{S35}$$

We can now choose $\beta = \frac{1}{8J}\ln\left[\frac{\kappa_{nn}+\kappa_1}{\kappa_1}\right]$ for some $\kappa_{nn}$. Then we have

$$\frac{\kappa_1}{2}\mathcal{D}(a_i + a_i^\dagger)[\rho_S] + \frac{\tilde{\kappa}_{nn}}{2}\sum_{\sigma(3)}\mathcal{D}((a_i + a_i^\dagger)P_{\sigma(3)})[\rho_S] + \frac{\kappa_{nn}}{2}\sum_{\sigma(4)}\mathcal{D}((a_i + a_i^\dagger)P_{\sigma(4)})[\rho_S], \tag{S36}$$

where $\tilde{\kappa}_{nn} = \sqrt{\kappa_1\kappa_{nn} + \kappa_1^2} - \kappa_1$. This is almost the same as the dissipators defined in Eq. (9) of the main text. The first difference is that all jumps here are proportional to $a_i + a_i^\dagger$, while in the main text all jumps are proportional to just $a_i$. (We shall address this in the next paragraph.) The second difference is that here $\kappa_1$ came solely from the bath that we designed ourselves, representing the fluctuations associated with a non-zero-temperature bath that disorders the state. We note that single-photon loss processes can also occur due to spontaneous emission for a single cavity, which arises due to processes that lower the energy within a single cavity (not included in the analysis above for

simplicity). Taking such terms into account amounts to shifting up the effective temperature of the model. However, as long as the composite system sits in the low-temperature part of the phase diagram (i.e. if the "zero-temperature" part of the bath is significantly stronger than the terms that generate bit flips), the system will sit in the part of the phase diagram that hosts a quantum memory.

To recover the photonic-Ising dissipators, we take into account the two-photon process on each photonic-Ising site. The two-photon process effectively constrains the bosonic Hilbert space on each site to a two-dimensional manifold, making the thermal equilibrium of $H_S$ well-defined. Without the two-photon process, $H_S$ is infinitely degenerate even for a finite photonic-Ising lattice, which leads to an ill-defined steady-state manifold for the Lindbladian even when detailed balance is enforced.

To simplify the analysis, we assume that $N = |\alpha|^2 \to \infty$ and $\kappa_2$ is nonzero, in which case the system is at all times close to the ideal manifold spanned by the two coherent states $|\pm\alpha\rangle = \left|\pm e^{-i\pi/4}\sqrt{N}\right\rangle$ with $\langle\alpha|-\alpha\rangle = 0$. So, within this two-dimensional Hilbert space, both $a$ and $a^\dagger$ have vanishing diagonal matrix elements, while their off-diagonal matrix elements are off by only a phase, so we can write $a + a^\dagger \to (1+i)a$. This finally yields

$$\kappa_1 \mathcal{D}(a_i)[\rho_S] + \tilde{\kappa}_{nn} \sum_{\sigma(3)} \mathcal{D}(a_i P_{\sigma(3)})[\rho_S] + \kappa_{nn} \sum_{\sigma(4)} \mathcal{D}(a_i P_{\sigma(4)})[\rho_S], \tag{S37}$$

which are the photonic-Ising dissipators [Eq. (9) in the main text] and the single-photon loss noise at site $i$.

Note that, while we made many assumptions to arrive at the precise dissipators from Eq. (9) in the main text, it is likely that nearly any low-temperature thermal Markovian bath will result in a protected quantum memory.

## 5. ENGINEERING AN ISING INTERACTION BETWEEN CAVITY MODES

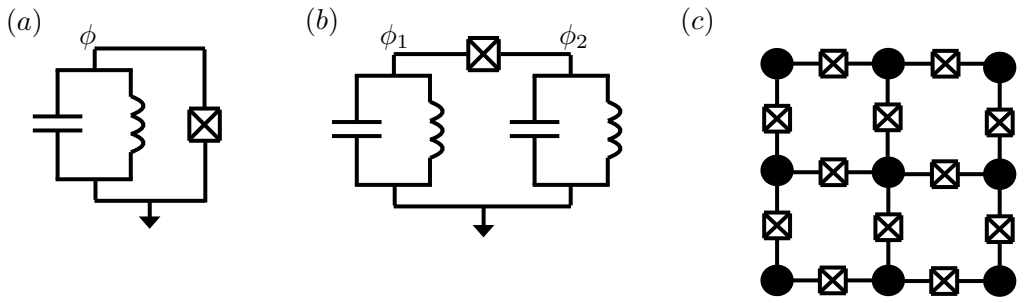


FIG. S5. (a) An $LC$ oscillator (representing a cavity) connected to a Josephson junction. The junction generates a Hamiltonian term that is proportional to the photon parity in the cavity. (b) Two $LC$ oscillators connected via a Josephson junction. The junction generates an Ising-like parity-parity interaction between the oscillators in a certain parameter regime. (c) Schematic layout for a 2D quantum memory: Black circles represent driven-dissipative resonator cavities (or $LC$ oscillators). Each resonator is coupled to its neighbor via a Josephson junction which generates an Ising-like interaction (in the appropriate limit).

We showed in the last section that the dissipators described in Eq. (9) most naturally appear as thermal dissipators corresponding to processes that raise and lower the energy of the Ising-like Hamiltonian $H = -J\sum_{\langle ij\rangle} Q_i Q_j$, where $Q_i = e^{i\pi a_i^\dagger a_i}$. The most straightforward approach to achieve a passively protected memory is therefore to engineer an Ising-like interaction between nearest-neighbor cat qubits. At low temperatures, the coupling of the system to its thermal environment can lead to thermal processes that drive the system to a ferromagnetic state, thus protecting the system against bit flips.

Previous studies have described how to achieve a parity-parity interaction term between neighboring cat qubits [4, 5]. Here we first review the steps needed to achieve a single-cavity Hamiltonian proportional to parity, closely following Ref. [4]. We then discuss the generalization to a parity-parity interaction which follows in a very similar manner.

Consider an LC oscillator (representing a cavity mode) connected to a Josephson junction, as shown in Fig. S5(a), in the presence of a two-photon drive on the cavity (not shown). The Hamiltonian of the system reads

$$H = \frac{\hat{q}^2}{2C} + \frac{\hat{\phi}^2}{2L} - E_J \cos\left(\hat{\phi}/\Phi_0\right) + \lambda\left(\hat{a}^2 e^{i\omega_d t} + (\hat{a}^\dagger)^2 e^{-i\omega_d t}\right), \tag{S38}$$

where $\hat{q}$ is the charge of the capcitor $C$, $\hat{\phi}$ is the flux through the inductor $L$, and $E_J$ is the Josephson energy, $\Phi_0 = \hbar/(2e)$ is the flux quantum, $\hat{a}$ annihilates an excitation of the cavity, $\lambda$ is the drive strength, and $\omega_d$ is the drive frequency. We note that the flux through the inductor is equal in magnitude to the flux through the Josephson junction since Kirchoff's law relates the voltage drop across the two elements at any given time. We can rewrite the Hamiltonian in terms of $a, a^\dagger$:

$$H = \hbar\omega(a^\dagger a + 1/2) - E_J \cos\left[x(a + a^\dagger)\right] + \lambda\left(a^2 e^{i\omega_d t} + (a^\dagger)^2 e^{-i\omega_d t}\right), \tag{S39}$$

where $\phi = \sqrt{\hbar Z/2}(a + a^\dagger), q = (1/i)\sqrt{\hbar/(2Z)}(a - a^\dagger), \omega = 1/\sqrt{LC}, Z = \sqrt{L/C}, x = \Phi_0^{-1}\sqrt{\hbar Z/2}$ and we drop the hats on operators henceforth.

Going to the interaction picture with respect to $\hbar\omega(a^\dagger a + 1/2)$, the Hamiltonian takes the form

$$H_{int} = -E_J \cos\left[x(ae^{-i\omega t} + a^\dagger e^{+i\omega t})\right] + \lambda(a^2 + (a^\dagger)^2) = -\frac{E_J}{2}(D[\beta(t)] + D[-\beta(t)]) + \lambda(a^2 + (a^\dagger)^2), \tag{S40}$$

where we have assumed an on-resonant drive, $\omega_d = 2\omega$, and defined the displacement operator $D[\beta(t)] = e^{\beta(t)a^\dagger - \beta^*(t)a}$, with $\beta(t) = ixe^{-i\omega t}$. We apply the rotating-wave approximation to remove all time dependence in the Hamiltonian, which is valid in the limit $\omega \gg E_J$:

$$H_{rw} = -E_J e^{-x^2/2} \sum_n \left(L_n(x^2)|n\rangle\langle n|\right) + \lambda(a^2 + (a^\dagger)^2), \tag{S41}$$

where $L_n$ is the Laguerre polynomial of order $n$.

The two-photon drive (along with engineered two-photon loss) ensures that the system is approximately confined to a two-dimensional manifold spanned by the cat states $|\alpha_e\rangle$ and $|\alpha_o\rangle$. In this subspace, the Hamiltonian is diagonal (since $H_{rw}$ is diagonal in the Fock basis). Further, if we set $x = 2|\alpha|$, then the Hamiltonian is exponentially close to the parity operator:

$$H_{rw}^{\text{cat}} = -\frac{\hbar\Omega}{2}(|\alpha_e\rangle\langle\alpha_e| - |\alpha_o\rangle\langle\alpha_o|) + O(E_J e^{-|\alpha|^2/2}) \tag{S42}$$

$$= -\left(\frac{\hbar\Omega}{2}\right) Q + O(E_J e^{-|\alpha|^2/2}), \qquad Q = e^{i\pi a^\dagger a}, \tag{S43}$$

where $\Omega = E_J/(\hbar\sqrt{2\pi|\alpha|^2})$. The exponentially small term is proportional to the identity in this subspace, which should not affect the dynamics.

Let us briefly summarize the physical conditions required to achieve a parity Hamiltonian of the form $H \sim Q$ in (S43) above. In the large $|\alpha|^2 \equiv N$ limit, we require that $E_J \sim \sqrt{N}$ such that the coefficient $\Omega$ does not tend to zero at large $N$. In order for the rotating wave approximation to be valid, we required that $\omega \gg E_J$. This implies that $\omega \sim \sqrt{N}$, which can be achieved with a small capacitance: $\omega \sim 1/\sqrt{LC}$ if $C \sim N^{-1}$. Finally, we required $x \sim \sqrt{L/C} \sim \sqrt{N}$. This is again satisfied with the small capacitance condition: $C \sim N^{-1}$.

So far, our discussion has focused on achieving a parity Hamiltonian for a single cavity. A very similar setup will result in a parity-parity interaction between neighboring cavity modes [4]. We briefly describe how this can be done.

Consider two driven LC oscillators which are connected to a Josephson junction, as shown in Fig. S5(b). (We again assume two-photon drives on each cavity as before, but neglect to include them in the Hamiltonian since they only serve the purpose of confining the state of the system to the cat state subspace, as described in the previous paragraphs.) The Hamiltonian for the system reads

$$H = \left(\frac{q_1^2}{2C_1} + \frac{\phi_1^2}{2L_1}\right) + \left(\frac{q_2^2}{2C_2} + \frac{\phi_2^2}{2L_2}\right) - E_J \cos(\phi_2 + \phi_1), \tag{S44}$$

where $\phi_{1/2}$ are the node fluxes defined in Fig. S5(b). Moving to the rotating frame of the cavity Hamiltonians leads to the interaction Hamiltonian

$$H_{int} = -E_J \cos\left((a_2 e^{-i\omega_2 t} + a_2^\dagger e^{i\omega_2 t}) + (a_1 e^{-i\omega_1 t} + a_1^\dagger e^{i\omega_1 t})\right), \tag{S45}$$

where $a_{1/2}$ are the annihilation operators associated with the two cavities, and $\omega_{1/2}$ are the frequencies. Applying the rotating-wave approximation leads to

$$H_{rw} = -E_J e^{-(x_1^2 + x_2^2)/2} \sum_{n_1, n_2} L_{n_1}(x_1^2) L_{n_2}(x_2^2)|n_1, n_2\rangle\langle n_1, n_2|. \tag{S46}$$

Note that we also require that the frequencies of the cavities should be incommensurate in order for the terms above to be the only ones that are time independent, i.e. $l_1\omega_1 \neq l_2\omega_2, \forall l_1, l_2 \in \mathbb{Z}$. Specializing to the two-dimensional cat state manifold leads to an interaction of the form

$$H_{rw}^{\text{cat}} = -\left(\frac{\Omega_1\Omega_2}{4E_J}\right) Q_1 Q_2, \qquad Q_{1/2} = e^{i\pi a_{1/2}^\dagger a_{1/2}}, \tag{S47}$$

where $\Omega_{1/2} = E_J/(\sqrt{2\pi|\alpha_{1/2}|^2})$ set the energy scale of the coupling between the two cavities $1, 2$.

Again, let us briefly summarize the physical conditions required to achieve the parity-parity Hamiltonian of the form $H \sim Q_1 Q_2$ in Eq. (S47) above. In the large $|\alpha|^2 \equiv N$ limit, we require that $E_J \sim N$ such that the coefficient $\sim \Omega_1\Omega_2/E_J$ does not tend to zero at large $N$. In order for the rotating wave approximation to be valid, we required that $\omega_{1/2} \gg E_J$ and $|\omega_1 - \omega_2| \gg E_J$. This implies that $\omega \sim N$. We also require that $x_{1/2} \sim \sqrt{L_{1/2}/C_{1/2}} \sim \sqrt{N}$. Both of these conditions can be achieved for $C_{1/2} \sim N^{-3/2}, L_{1/2} \sim N^{-1/2}$.

A schematic layout for a 2D quantum memory is provided in Fig. S5(c): Each black dot represents a driven-dissipative resonator, connected to its neighbor via a Josephson junction that results in an Ising interaction. The advantage of the passive approach is the lack of ancilla qubits and of precise pulse signals that are typically needed to make the measurements required for active error correction. The passive approach also avoids the need for classical communication with a decoder.

Let us briefly estimate the logical decoherence rate for a model with $N = 30, M = 10$, composed of state-of-the-art circuit elements. The logical bit-flip time for a single photonic cavity is set by the single-photon loss rate, which is about $\kappa_1/2\pi = 20$ kHz [6]. [Note that our naming convention for bit/phase-flip errors differs from the conventional cat qubit literature.] For a cavity with $N$ photons, this rate increases to $N\kappa_1/2\pi = 20N$ kHz, corresponding to a logical bip-flip time of about 1.6 $\mu$s for $N = 30$. Placing such cat qubits on an $M \times M$ lattice for $M = 10$, and assuming that $\beta = 0.49$, we see (from Fig. 2) that the logical bit-flip time gets improved by a factor of $10^3$, suggesting an overall logical bit-flip time of about 1.6 ms. We can similarly estimate the logical phase-flip time: A single cavity with $N = 30$ has a logical phase-flip time of about 1 s [6]. Constructing an $M \times M$ lattice of such cavities leads to an overall logical phase-flip time of $1/10^2$ s $= 10$ ms. We therefore find that such a system is expected to have both a bit-flip and phase-flip time that exceeds 1 ms. In terms of circuit parameters, the Ising coupling strength is set by $J = E_j/(8\pi N)$. For $E_j/2\pi = 400$ GHz and $N = 30$, we can achieve an effective $\beta = 0.49$ if the physical temperature is $T = 51$ mK, which can be achieved via standard dilution refrigerators.

A major challenge of constructing such a model involves realizing a high-impedance cavity mode. The condition $x = 2|\alpha|$ implies that the impedance of the cavity should satisfy $Z = 8NR_Q$, where $R_Q$ is the resistance quantum. Currently, superimpedances constructed out of Josephson junction arrays have reached about $Z = 8R_Q$ [4], so achieving such a high impedance will be challenging for $N = 30$. Nevertheless, we note that, in principle, the impedance can be made arbitrarily large by increasing the number of Josephson junctions in the array. We also note that the capacitance can be made arbitrarily small by connecting capacitors in series.

It is also challenging to meet the rotating-wave approximation in the model described above: The proposed model would require cavities with frequencies on the order of a few terahertz in order to meet both $\omega \gg E_j$ and $|\omega_1 - \omega_2| \gg E_j$, with $E_j/2\pi = 400$ GHz. Superconducting microwave resonators are defined to have a frequency in the range of 300 MHz to 300 GHz, so terahertz resonators are beyond the microwave regime. High resonator frequencies would cause excitations to have energies that are larger than the superconducting gap of standard materials (around 20 GHz for aluminum), leading to the loss of superconductivity via the breakup of Cooper pairs. Exotic superconductors might help reach such high resonator frequencies [7].

We also note the following two points. (i) We quoted the sufficient condition under which the rotating-wave approximation is valid, but in practice the validity of the approximation might be more general. The approximation is applied to the Hamiltonian of the form $\sim \omega a^\dagger a + E_j \cos\big(x(a^\dagger + a)\big)$. When the cavity contains a non-trivial number of bosons, the first term always dominates over the $E_j$ coupling, allowing for a perturbative treatment even when the above condition is not met. A promising path for future work is to investigate to what extent the condition can be relaxed. (ii) Future efforts to design a circuit QED realization of this model might be able to avoid the rotating-wave approximation by working with a *non-driven* protected qubit (instead of cat qubits). For example, the zero-pi qubit [8] has an exponentially-long $T_1$ time as a function of circuit parameters, while its $T_\phi$ time is generally nonzero when circuit disorder is taken into account. The logical dephasing rate could be exponentially suppressed by engineering an Ising interaction between a 2D lattice of zero-pi qubits (or other protected qubits), which could be done in the lab frame (i.e. without a rotating-wave approximation) thus providing another route towards realizing the passive memory that might be less challenging for experimental designs.

The scheme we have just described to achieve a parity-parity interaction requires fabricating a device with challenging circuit requirements, as outlined above. Nevertheless we emphasize that this proposal suggests an exponential

suppression of errors at only a polynomial increase of resources (i.e. energy scales and lattice sites). It is conceivable that there are other routes towards achieving similar passive 2D memories that are not as demanding to realize. The field of superconducting circuits potentially provides new routes to achieve such a model. In particular, certain qubits can achieve exponential suppression of errors as a function of circuit parameters, e.g. squeezed cat qubits [9–11], Kerr qubits [12, 13], $\cos(2\theta)$ qubits, and zero-pi qubits [14–16]. Future work should investigate ways to achieve an Ising interaction for different types of protected qubits. We hope that the theoretical model for a passively corrected quantum memory that we propose (a 2D lattice of harmonic oscillators) can motivate improved experimental designs (with circuit QED or other platforms) which address the mentioned challenges.

Let us also briefly comment on the possibility of doing initialization, readout, and gates on our proposed quantum memory (closely following Ref. [17], which uses a different basis convention). If we start with all cavities in the vacuum state, then turn on the coherent two-photon drive and the incoherent two-photon loss, we will initialize the system in the logical 0 state: $|\bar{0}\rangle = |\alpha_e\rangle|\alpha_e\rangle|\alpha_e\rangle\ldots$. For readout in the $|\bar{0}\rangle/|\bar{1}\rangle$ basis (where $|\bar{1}\rangle = |\alpha_o\rangle|\alpha_o\rangle|\alpha_o\rangle\ldots$), we rely on a dispersive parity measurement: We can turn on a dispersive interaction between the data qubit and a transmon ancilla (e.g. mediated by a coupler), to achieve the effective Hamiltonian $H_{disp} = \chi|e\rangle\langle e|a^\dagger a$. Evolving for a time $T = \pi/\chi$ leads to the unitary $U = |g\rangle\langle g|I + |e\rangle\langle e|\exp\left[i\pi a^\dagger a\right]$. Initializing the ancilla in $(|g\rangle + |e\rangle)/\sqrt{2}$ means that the unitary will only evolve to $(|g\rangle - |e\rangle)/\sqrt{2}$ if the parity of the cavity is odd. Doing a standard X measurement of the transmon will thus distinguish the parity of the cavity. We measure all cavity parities and take the majority vote to infer logical 0 or 1.

The X gate can be engineered by keeping, for every cavity, the two-photon drive and two-photon loss on and applying an additional coherent single-photon drive Hamiltonian $\sim \epsilon(a + a^\dagger)$ for time $T = \pi/(2\epsilon|\alpha|)$. The Z gate can be done by choosing a single cavity and adiabatically tuning the phase on the coherent two-photon drive process: $\lambda e^{i\theta(t)}a^2 + h.c.$, where $\theta(t)$ is adiabatically tuned from 0 to $\pi$. This will "swap" the states $|+\alpha\rangle$ and $|-\alpha\rangle$ on that cavity, which is equivalent to applying a $\pi$ phase on state $|\alpha_o\rangle$ on that cavity, which is in turn equivalent to a logical $Z$ gate on the logical space defined by $|\bar{0}\rangle = |\alpha_e\rangle|\alpha_e\rangle|\alpha_e\rangle\ldots$ and $|\bar{1}\rangle = |\alpha_o\rangle|\alpha_o\rangle|\alpha_o\rangle\ldots$. Ref. [17] goes on to define bias preserving logical CNOT gates and Toffoli gates for cat qubits (CZ and CCZ gates in our basis convention), which lead to a universal set of bias-preserving, fault-tolerant gates that can be done on the 1D active repetition cat code. Our analysis suggests that the repetition cat code can be done fully passively via the Ising interaction on a 2D lattice. We do not see any reason why these gate schemes should not work in an analogous passive scheme although future work should look into this in more detail. We note that previous studies suggest that universal gates can be done transversally on a passive quantum memory, but the system lives in seven dimensions or above, e.g. the 7D color code [18, 19].

While bias-preserving gates are in general more challenging (and often slower) to implement than non-bias preserving ones, we note that, in a fully passive scheme, the only gates we need to apply are logical gates. Specifically, we do not need extremely fast gates between data and ancilla required to meet the threshold for active error correction. So some of the usual speed requirements on two-qubit gates could potentially be relaxed in the passive scheme. The only speed condition that we need to meet is that the logical gate times should be much shorter than the coherence times.

## 6. DIGITAL AUTONOMOUS PHOTONIC-ISING LOCAL DECODER

In this section, we describe a digital autonomous approach for realizing a stochastic local error decoder inspired by the photonic-Ising dissipators defined in the main text. This procedure involves implementing a sequence of fault-tolerant local gates to correct the errors without the need of measurements. The step is then iterated over time on the entire system as fast as possible. Although this approach is different from directly realizing the microscopic Lindbladian (which could be done by dividing the error-correcting step infinitesimally [20, 21]), this digital approach is potentially easier to realize experimentally, and we expect that it provides the same dynamical protection of the quantum memory. Note that the protocol requires the rate of the digital steps to scale linearly with the average photon number.

It suffices to consider the implementation of the local decoder at a single time step. Consider a square lattice of photonic cavities. Over each lattice cavity, we place an ancillary cavity (initialized in $|\alpha_o\rangle$).

We describe the implementation at a single site and the generalization to the whole lattice follows straightforwardly. First, for a given site, we perform an encoding unitary $U$. Depending on the state of the chosen lattice cavity and its four neighbors, $U$ changes the state of the ancillary cavity via

$$U = P \otimes (|\alpha_e\rangle\langle\alpha_o| + |\alpha_o\rangle\langle\alpha_e|) + P^\perp \otimes (|\alpha_o\rangle\langle\alpha_o| + |\alpha_e\rangle\langle\alpha_e|), \tag{S48}$$

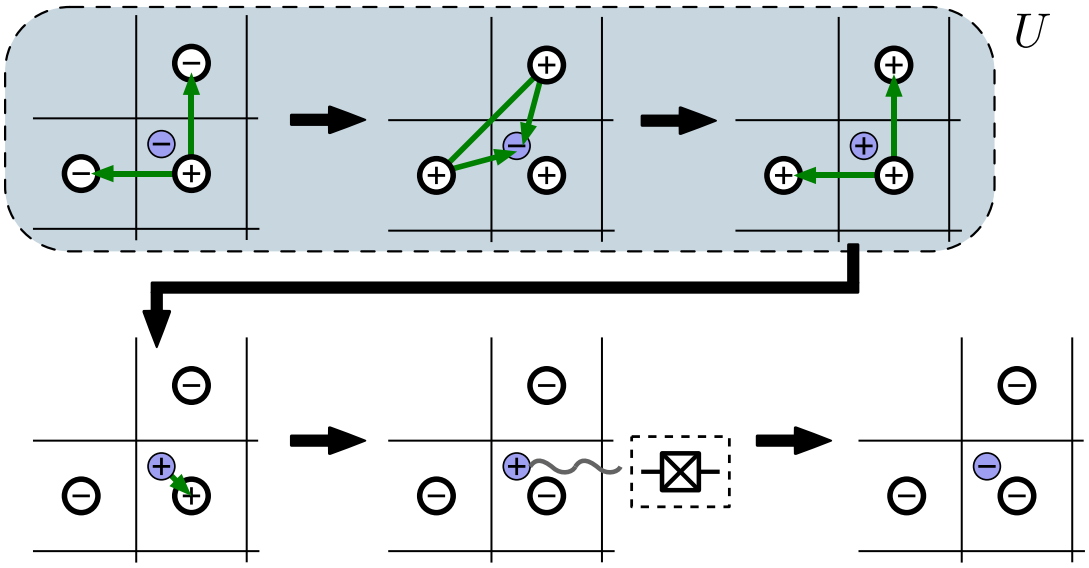


FIG. S6. Illustration of the digital autonomous photonic-Ising local decoder when $U$ is implementing Toom's rule. Purple color labels the ancillary cavity. We denote $|\alpha_o\rangle$ by $(-)$ and $|\alpha_e\rangle$ by $(+)$. The green arrows are CNOT gates, pointing from the control cavity to the target cavity. A connected double green arrow is a Toffoli gate. The procedure consists of the following steps: (i) two CNOTs from the central cavity to its neighbors; (ii) a Toffoli gate from the neighbors to the ancillary cavity; (iii) two CNOTs from the central cavity to its neighbors; (iv) a CNOT from the ancillary cavity to the central cavity; (v) reset the ancillary cavity via coupling to a transmon.

where $P$ projects on a local configuration of domain walls (a specific example was considered in the main text, where we project onto a configuration with 3 or 4 misaligned neighboring lattice cavities) and $P^\perp$ is the orthogonal subspace projector. We define the unitary $U$ such that it changes the ancillary cavity from $|\alpha_o\rangle$ to $|\alpha_e\rangle$ if a local error is detected; it does nothing otherwise. Note that $U$ can be implemented using the fundamental set of bias-preserving gates in Ref. [17], where the two-photon drive and two-photon loss can be kept on thus suppressing the dephasing errors during the gate implementation.

Second, we apply a CNOT gate (described in Section IV.D in Ref. [17]) that is controlled by the ancillary cavity and targets the corresponding lattice cavity. (We use the convention that $|\alpha_o\rangle$ is $|0\rangle$ and $|\alpha_e\rangle$ is $|1\rangle$).

Third, we use a strong dispersive coupling to a transmon to extract the entropy from the ancillary cavity [22] and reset it back to the initial state $|\alpha_o\rangle$. Due to the fault-tolerance of the cavity-cavity gates [17], the phase errors stay suppressed when the Ising-type local decoder is implemented autonomously.

The full procedure is achieved by implementing the encoding and the reset across the entire lattice. To extend the single-site procedure to the entire lattice, we note that the encoding operations $U$ on each site are local around each lattice cavity and they commute across different lattice sites. Therefore, the encoding $U$ can be implemented in parallel across all the sites before a final reset, e.g. by dividing the lattice into bipartite sublattices and operating on the cavities that belong to the same sublattice in parallel.

For concreteness, let us consider an example where $U$ flips the ancillary cavity if it identifies a corner formed by the domain walls, i.e. Toom's rule. (Digitally, this is simpler than the majority rule described in the main text, but one could implemenent the majority rule approach as well.) Then $U$ for a chosen orientation can be implemented by the following gate sequence

1. Apply two CNOTs from center lattice cavity to its neighboring cavities on the left and on the top.

2. Apply a Toffoli gate (described in Section IV.E in Ref. [17]) controlled by the two neighboring cavities and targeting the ancillary cavity.

3. Repeat step 1 to invert the two CNOTs applied.

The digital procedure for the autonomous implementation of Toom's rule on a particular configuration is schematically depicted in Fig. S6.

The autonomous approach above can be easily turned into an active error correction protocol: instead of applying a CNOT from the ancillary cavity to the central cavity and then resetting the ancillary cavity, we can measure

the ancillary cavity and flip the parity of the central cavity if the measurement result is (+). Alternatively, when implementing active error correction, we can place a syndrome cavity between each pair of neighboring cavities on the lattice. By storing in the syndrome cavity the information regarding the presence of a domain wall, we can implement a local decoder based on the rules defined by $U$. This then becomes a 2D version of a repetition cat code. Again, all the steps can be achieved with dephasing errors exponentially suppressed. In contrast with the non-local processing of syndrome information required by the 1D repetition cat code in Ref. [17], the 2D code allows for a stochastic local decoding procedure. As mentioned at the beginning of the section, to achieve an exponentially long memory time, both the autonomous and the active error correction approaches require scaling the rate of the digital step linearly with the average number of cavity photons $N$ because bit-flip error rate scales with $N$.


[1] C. Chamberland, K. Noh, P. Arrangoiz-Arriola, E. T. Campbell, C. T. Hann, J. Iverson, H. Putterman, T. C. Bohdanowicz, S. T. Flammia, A. Keller, G. Refael, J. Preskill, L. Jiang, A. H. Safavi-Naeini, O. Painter, and F. G. Brandão, PRX Quantum **3**, 010329 (2022).
[2] S. Lieu, R. Belyansky, J. T. Young, R. Lundgren, V. V. Albert, and A. V. Gorshkov, Phys. Rev. Lett. **125**, 240405 (2020).
[3] H. Breuer and F. Petruccione, *The Theory of Open Quantum Systems* (Oxford University Press, 2002).
[4] J. Cohen, W. C. Smith, M. H. Devoret, and M. Mirrahimi, Phys. Rev. Lett. **119**, 060503 (2017).
[5] J. Cohen, *Autonomous quantum error correction with superconducting qubits*, Ph.D. thesis, Ecole Normale Superieure (2017).
[6] C. Berdou, A. Murani, U. Reglade, W. Smith, M. Villiers, J. Palomo, M. Rosticher, A. Denis, P. Morfin, M. Delbecq, *et al.*, arXiv preprint arXiv:2204.09128 (2022).
[7] A. Schilling, M. Cantoni, J. D. Guo, and H. R. Ott, Nature **363**, 56 (1993).
[8] P. Brooks, A. Kitaev, and J. Preskill, Phys. Rev. A **87**, 052306 (2013).
[9] D. S. Schlegel, F. Minganti, and V. Savona, Phys. Rev. A **106**, 022431 (2022).
[10] T. Hillmann and F. Quijandría, Phys. Rev. A **107**, 032423 (2023).
[11] Q. Xu, G. Zheng, Y.-X. Wang, P. Zoller, A. A. Clerk, and L. Jiang, npj Quantum Inf. **9**, 78 (2023).
[12] B. Yurke and D. Stoler, Phys. Rev. Lett. **57**, 13 (1986).
[13] A. Grimm, N. E. Frattini, S. Puri, S. O. Mundhada, S. Touzard, M. Mirrahimi, S. M. Girvin, S. Shankar, S. Shankar, and M. H. Devoret, Nature **584**, 205 (2020).
[14] P. Brooks, A. Kitaev, and J. Preskill, Phys. Rev. A **87**, 052306 (2013).
[15] B. Douçot and L. B. Ioffe, Reports on Progress in Physics **75**, 072001 (2012).
[16] A. Gyenis, A. Di Paolo, J. Koch, A. Blais, A. A. Houck, and D. I. Schuster, PRX Quantum **2**, 030101 (2021).
[17] J. Guillaud and M. Mirrahimi, Phys. Rev. X **9**, 041053 (2019).
[18] H. Bombin, R. W. Chhajlany, M. Horodecki, and M. A. Martin-Delgado, New Journal of Physics **15**, 055023 (2013).
[19] A. Kubica and M. E. Beverland, Phys. Rev. A **91**, 032330 (2015).
[20] H. Weimer, M. Müller, I. Lesanovsky, P. Zoller, and H. P. Büchler, Nat. Phys. **6**, 382 (2010).
[21] J. T. Barreiro, M. Müller, P. Schindler, D. Nigg, T. Monz, M. Chwalla, M. Hennrich, C. F. Roos, P. Zoller, and R. Blatt, Nature **470**, 486 (2011).
[22] Z. Leghtas, G. Kirchmair, B. Vlastakis, R. J. Schoelkopf, M. H. Devoret, and M. Mirrahimi, Phys. Rev. Lett. **111**, 120501 (2013).